Water Resources Research

RESEARCH ARTICLE
10.1029/2023WR036877

Effects of Initial Injection Condition on Colloid Retention

Bashar M. Al-Zghoul[1], Sabrina N. Volponi[1], W. P. Johnson[2], and Diogo Bolster[1]

[1]Department of Civil & Environmental Engineering & Earth Sciences, University of Notre Dame, Notre Dame, IN, USA, [2]Department of Geology & Geophysics, University of Utah, Salt Lake City, UT, USA

Key Points:

- The study finds that initial injection conditions strongly influence colloid transport and retention profiles
- Different injection methods lead to varied retention patterns, revealing insights into anomalous transport in porous media
- The findings underscore the importance of injection conditions in experimental design to better understand colloid transport behavior

Correspondence to:
B. M. Al-Zghoul,
balzghou@nd.edu

Citation:
Al-Zghoul, B. M., Volponi, S. N., Johnson, W. P., & Bolster, D. (2024). Effects of initial injection condition on colloid retention. *Water Resources Research*, *60*, e2023WR036877. https://doi.org/10.1029/2023WR036877

Received 8 DEC 2023
Accepted 20 MAY 2024

Abstract This study investigates the impact of initial injection conditions on colloid transport and retention in porous media. Employing both uniform and flux-weighted distributions for the initial colloid locations, the research explores diverse flow scenarios, ranging from simple Poiseuille flow to more complex geometries. The results underscore the pivotal role the injection mode plays on the shape of colloid retention profiles (RPs), particularly those that display anomalous non-exponential decay with distance. Broadly, uniform injection yields multi-exponential profiles, while flux-weighted injection can lead to nonmonotonic profiles in certain conditions. The study identifies preferential flow paths as a key factor in producing nonmonotonic RPs. Notably, variations in fluid velocity, colloid size, and ionic strength affect attachment rates near the inlet but do not significantly alter the qualitative transition between multi-exponential and nonmonotonic profiles. The study emphasizes that the chosen injection mode dictates retention profile shapes, highlighting its crucial role in porous media colloid transport. These insights provide a possible partial explanation of previously observed anomalous transport behaviors, urging consideration of injection conditions in interpretations of experiments, where they can be difficult to accurately control and measure with high precision.

1. Introduction

Migration of colloidal particles, which typically range in size from 10 nm to 10 μm, within the subsurface environment is a topic of significant interest. Important examples include the transport of pathogens (e.g., viruses and bacteria), heavy metals (e.g., lead, mercury, and cadmium), organic colloids (e.g., pesticides, herbicides, and pharmaceuticals), and engineered nanoparticles (ENPs) through groundwater, as it can impact water quality and human health (Al-Zghoul & Abu-El-Sha'r, 2020; Deb & Chakma, 2022; Klaine et al., 2008; Petosa et al., 2010). Transport of colloids relative to other substances is complex due to a variety of physio-chemical interactions between the colloids and porous media surfaces that can cause particles to be retained on solid boundaries. One challenge lies in accurately predicting retention profiles (RPs) of colloids, that is, the number of colloids that become attached to the surface of the hosting medium as a function of distance from the source. Accurately predicting RPs serves as a key indicator of the contaminant's spread within a system, playing a crucial role in evaluating and mitigating the risks associated with its transport (Molnar et al., 2015).

To date, several mechanistic models have been developed to predict colloid and nanoparticle transport (Nelson & Ginn, 2011; Rajagopalan & Tien, 1976; Tufenkji & Elimelech, 2004a). These typically rely on applying force and torque balances to accurately characterize the trajectories of individual colloids, often within the Happel sphere-in-cell model, an idealized representation of a flow in a porous medium. These models incorporate a range of relevant forces, encompassing both physical (such as fluid drag, diffusion, virtual mass, and gravity) and physicochemical forces (including van der Waals (VDW) and electric double layer (EDL) interactions as delineated by DLVO theory) (Derjaguin & Landau, 1941; Verwey & Overbeek, 1948), which govern the process of colloidal migration and attachment to surfaces. Like-charged colloid and collector surfaces generate a repulsive EDL force, associated with unfavorable conditions, which prevents the colloid from passing the secondary minimum and making contact with the collector. Under such circumstances one would expect no attachment to occur, yet experimental evidence demonstrates that it does (Ellmelech & O'Mella, 1990). A potential explanation for observing attachment under unfavorable conditions is the presence of local surface heterogeneity on the collector grains of the medium that have localized zones with the opposite charge to the colloid (Ryan & Elimelech, 1996). To better predict attachments under such conditions, nanoscale discrete attractive zones called heterodomains were introduced on the surface of collectors and employed in mechanistic pore-scale simulation on Happel sphere-in-cell collector (Pazmino, Trauscht, Dame, & Johnson, 2014; Pazmino, Trauscht, & Johnson, 2014; Trauscht et al., 2015).

Colloid filtration theory (Yao et al., 1971) has traditionally been employed to describe the RPs of colloids in porous media using a simple single linear rate (exponential removal) model. It has proven effective in characterizing RPs under favorable conditions, where forces between colloids and the collector grains are attractive. However, several studies (X. Li et al., 2004; Tong & Johnson, 2007; Tufenkji & Elimelech, 2004b) have shed light on the inherent limitations of this conventional approach when confronted with unfavorable conditions. In specific scenarios and under unfavorable conditions, the shape of RPs can manifest as multi-exponential (characterized by a rapid initial decrease followed by a slower decline) or nonmonotonic (featuring a rapid initial increase followed by a decrease). These profile shapes serve to highlight the anomalous nature of colloid migration process. Several experimental studies on colloid transport in porous media under unfavorable conditions have observed both multi-exponential and nonmonotonic RPs. Multi-exponential RPs were first observed for bacteria (Albinger et al., 1994), nonbiological material such as carboxylate-modified-polystyrene latex microspheres (CML) (X. Li et al., 2004; Tong & Johnson, 2007; Tufenkji & Elimelech, 2004b), and ENPs (Liang et al., 2013). Similarly, nonmonotonic RPs were seen in experiments with CML microspheres, biological, and nanosized colloids (Tong et al., 2005; Wang et al., 2014). To better understand this anomalous behavior, (X. Li et al., 2004) conducted experiments on the transport of CML colloids through a glass bead pack under a variety of environmentally relevant ionic strength (IS) and flow conditions and observed multi-exponential RPs under unfavorable conditions. On the other hand, identical colloids (CML) displayed non-monotonic RPs when tested in quartz sand packs (X. Li & Johnson, 2005). Johnson et al. (2018) explained the observation of both multi-exponential and nonmonotonic RPs via differences in colloid residence times in the near surface fluid domain before attachment on grains. These differences can be effectively modeled using a multi-continuum model where colloids migrate "rapidly" through the bulk flow and either attach directly to the surface or move to a much slower near-surface zone (NSZ) where they can slowly migrate over significant times before being retained. Under such circumstance the residence time of a colloid before attachment is characterized by the sum of two exponential distributions, one from the bulk to the near surface and the other from the near surface to the surface. The distribution of the sum of two exponentially distributed random variables is a hypo-exponential or generalized Erlang distribution (Amari & Misra, 1997), which can explain the multi-exponential and non-monotonic RPs.

The shape of RPs can be influenced by a range of properties including the properties of the colloids themselves (e.g., colloid size and density), the characteristics of the fluid (e.g., IS, viscosity, density, and temperature), the hosting medium geometry (e.g., grain angularity, length, and number of grain-to-grain contacts), and flow conditions. However, one effect that is difficult to control in experiments and not well studied to date is the role of the initial conditions of colloids (i.e., where they start in the flow field) that can considerably affect transport (X. Li & Johnson, 2005; X. Li et al., 2004). Several studies shed light on the effect of initial conditions for conservative transport in the context of micro and field scales both in fractured (Frampton & Cvetkovic, 2009, 2011; Hyman & Dentz, 2021; Hyman et al., 2015; Kang et al., 2017) and porous media (Comolli et al., 2019; Demmy et al., 1999; Gotovac et al., 2009, 2010; Puyguiraud et al., 2019a, 2019b). In particular, differences are observed when considering two end-member initial conditions: (a) uniform (or resident) injection and (b) flux-weighted. Real experimental conditions likely lie somewhere between these two. We argue that such effects are likely as, if not more important in the context of colloid transport, particularly given that diffusion of colloids is orders of magnitude slower than for solutes meaning that initial condition effects persist for longer (Taylor, 1953).

Several mathematical models have been developed to capture multi-exponential and nonmonotonic RP shapes (Bradford et al., 2006, 2011; Malgaresi et al., 2019; Shapiro & Bedrikovetsky, 2008; Yuan & Shapiro, 2010, 2011). Yuan and Shapiro (2010) proposed an integral analytical model of the deep bed filtration process that explains the observation of multi-exponential RPs in complex porous media by considering particle populations in connection with the distribution of filtration coefficients, heterogeneity in connection with non-Fickian transport, and heterogeneity in connection with the spatial distribution of filtration coefficients. Yuan and Shapiro (2011) also proposed a mathematical model to capture nonmonotonic RPs by considering model parameters based on near-surface interactions. Malgaresi et al. (2019) explained the occurrence of nonmonotonic and multi-exponential RPs by considering particle-size dependency of attachment areas on grain surfaces. They used a mathematical model to analyze colloid retention for small and large colloid sizes, noting the difference in attachment probability. Larger particles are rapidly retained near the inlet due to higher capture probabilities, while smaller particles persist further into the domain. Competition for surface vacancies shifts retention patterns over time, with larger particles increasingly retained near the inlet, resulting in elevated retention rates for both sizes. Small particles often exhibit non-monotonic profiles, with maximum concentrations at a specific point in

the flow direction, while large particle retention typically decreases monotonically. Ultimately, all RPs stabilize, displaying multi-exponential or non-monotonic behavior depending on particle size and the attachment area. Even though this can be one of the reasonable explanations for observing multi-exponential and nonmonotonic RPs, the anomalous transport in colloid can be observed also among identical individuals (Johnson et al., 2018; X. Li & Johnson, 2005; X. Li et al., 2004). In this study, we focus primarily on studying anomalous transport among identical individuals rather than rather than examining variations in colloid sizes.

In this paper, we utilize mechanistic pore-scale trajectory simulations to investigate the retention of colloids in a hierarchy of increasingly complex flows representative of porous media. The objective is to analyze the impact of initial injection conditions on colloid transport behavior. Two injection modes, uniform and flux-weighted, are tested across a range of colloid sizes, fluid velocities, and ionic strengths under favorable and unfavorable conditions. We conduct these simulations to address the following questions: (a) Can we observe "anomalous" multi-exponential and nonmonotonic RPs, merely by altering the initial injection condition? (b) How do parameters such as colloid size, IS, and fluid velocity influence this? And (c) Are multi-exponential and nonmonotonic RPs unique for unfavorable conditions, as commonly observed to date, or can they emerge under favorable conditions also?

2. Methodology

In this paper, we employ mechanistic Lagrangian particle tracking simulations in 2D pore-scale flows to highlight the effect of the initial condition on colloid transport behavior. Generally, pore-scale flow is governed by the Navier-Stokes equation. We simulate the flow under steady-state conditions at low Reynolds numbers, that is, $\mathrm{Re} = v_c l_c/\nu < 1$ with a characteristic velocity and length v_c and l_c, respectively, and kinematic viscosity ν. While we expect inertial conditions to be negligible, rather than only solving the Stokes equation for creeping flow, we employ the full steady-state Navier-Stokes equation

$$\boldsymbol{v}\cdot\nabla\boldsymbol{v} = -\frac{1}{\rho}\nabla p + \nu\nabla^2\boldsymbol{v}, \tag{1}$$

where p is the fluid pressure, ρ the fluid density, and $\boldsymbol{v}$ is the Eulerian fluid velocity. Details of the flow boundary conditions for our different flows are discussed in Section 2.1 below. We consider Newton's second law to obtain the colloid Lagrangian velocity $\boldsymbol{u}$,

$$(m_p + m^*)\,\frac{du(t,\boldsymbol{x})}{dt} = F_D + F_B + F_{EDL} + F_{VDW} \tag{2}$$

Where $m_p = \frac{1}{6}\pi d_p^3 \rho_p$ denotes a spherical colloid's mass with diameter d_p and density ρ_p, m^* is the virtual mass (the mass of one-half of the displaced fluid volume of the colloid (Gondret et al., 2002)), and the terms on the right-hand side of the equation are the forces acting on the colloid. These forces include fluid drag (F_D), Brownian force (F_B), electric double-layer ($F_{E\,DL}$), and van der Waals ($F_{V\,DW}$), with expressions of these forces provided in Ma et al. (2009). Gravitational forces are neglected; our simulations are in two-dimensions so this is reflective of a horizontal plane.

We consider two initial distributions of the colloids at the inlet $\rho(\boldsymbol{x_o})$. The uniform injection condition places particles equidistant from each other along an injection line. This gives

$$\rho(\boldsymbol{x_o}) = \frac{\mathbb{I}_{\psi_o}(\boldsymbol{x_o})}{V_o} \tag{3}$$

where ψ_o is the injection domain and V_o its volume. $\boldsymbol{x_o}$ denotes initial particle location and the indicator function, $\mathbb{I}_{\psi_o}(\boldsymbol{x_o})$, is equal to 1 if $\boldsymbol{x_o} \in \psi_o$ and 0 otherwise. The flux-weighted injection condition distributes particles in proportion to their initial velocity ($v_o(\boldsymbol{x_o})$) as

$$\rho(x_o) = \frac{v_o(\boldsymbol{x_o})\,\mathbb{I}_{\psi_o}(\boldsymbol{x_o})}{\int_{\psi_o} v_o(\boldsymbol{x_o})\,d\boldsymbol{x_o}} \tag{4}$$

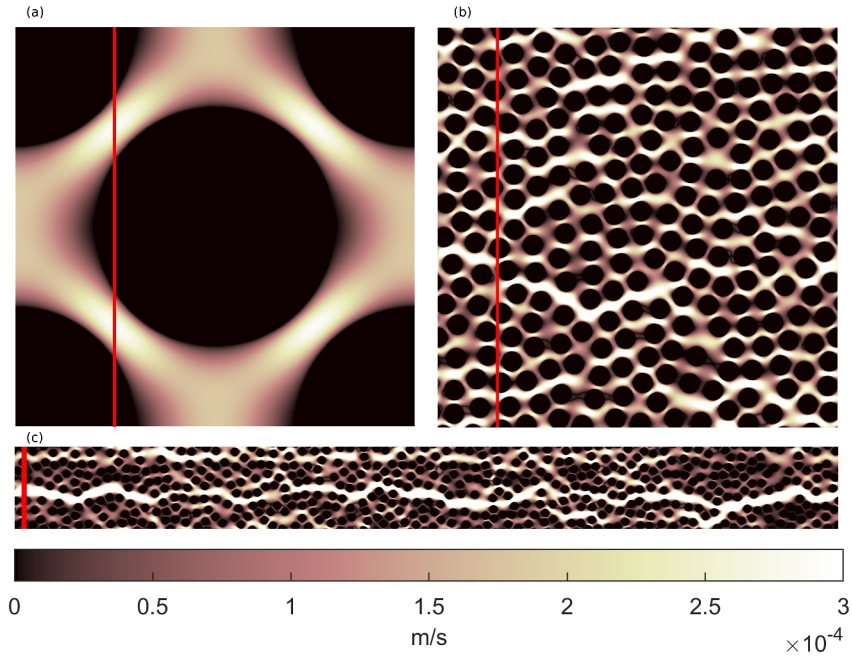

Figure 1. Simulated velocity field using OpenFOAM at $\langle \boldsymbol{v} \rangle \approx 8$ m/day using periodic boundary conditions in both directions (the mean flow direction is from left to right). The fluid domain along the red line indicates the injection location. (a) Homogeneous symmetrical geometry illustrates an idealized flow pattern around five symmetrical collectors, each measuring 300 μm in size, positioned at the center and corners of the domain, with a system porosity of 0.43. (b) Complex geometry with uniform collector size (200 μm) and porosity of 0.53 provides a more realistic representation of porous media. (c) Complex geometry with introduced preferential flow pathways emphasizes the contrast between high and low flux zones, maintaining a uniform collector size of 200 μm and a porosity of 0.55.

This injection mode places more colloids in the high-flux regions rather than distributing them uniformly or randomly. Both injection modes consider a finite number of colloids injected as a pulse.

2.1. Flow and Numerical Domains

2.1.1. Poiseuille's Flow

We first consider the simple example of Poiseuille flow, that is flow between two parallel plates, to answer our question on the effect of the initial condition on the colloid deposition. The solution of Equation 1 considering a channel width of 2d and boundary conditions of $\boldsymbol{v}(y = \pm d) = 0$ (no slip at the walls) provides

$$v(y) = 1.5\langle \boldsymbol{v} \rangle \left(1 - \left(\frac{y}{2d}\right)^2\right) \qquad -d \le y \le d, \tag{5}$$

where y is normal to the flow direction and $\langle \boldsymbol{v} \rangle$ is the average fluid velocity. Flow is assumed to be fully developed along the flow direction x. This provides a fluid velocity vector, $\boldsymbol{v}(x, y, z) = [v(y)\ 0\ 0]$, valid everywhere inside the channel. This flow is often considered an idealized representation of flow in a porous medium (De Anna et al., 2017), although it certainly lacks many important features such as tortuosity.

2.1.2. Flow in Periodic Porous Media

Next we focus on a simple 2D homogeneous symmetric geometry and more complex 2D geometries. The homogeneous geometry, Figure 1a consists of a domain containing multiple grains, each with a diameter of 300 μm. To maintain symmetry, one grain is positioned at the center, while the remaining four are evenly distributed at the corners. The domain itself measures 500 × 500 μm and possesses a porosity of 0.43. For the more complex geometries, we used the collision-driven packing generation algorithm to generate periodic geometries as displayed in Figures 1b and 1c (Skoge et al., 2006). The main difference between these domains (Figures 1b and 1c)

is that the geometry in Figure 1c has more pronounced preferential flow pathways. The domain size in Figure 1b is 4,000 × 4,000 μm. It consists of 200 μm grains with a porosity of 0.53. The domain in Figure 1c has 200 μm grains with a porosity of 0.55 and a domain size of 20,000 × 2,000 μm. In all domains, flow is solved using OpenFOAM, an open source community supported computational fluid dynamics software package (Christopher, 2022). By employing the SIMPLE algorithm within OpenFOAM, we solve the Navier-Stokes equation to obtain the velocity field. We specify the Eulerian mean velocity (average velocity) $\langle \boldsymbol{v} \rangle$ of the domain. A no-slip condition is enforced on the grain surfaces. Additionally, cyclic (periodic) boundary conditions are implemented on the domain faces. The mean flow direction is from left to right, aligned with the positive x-axis. Figure 1 shows the velocity field for $\langle \boldsymbol{v} \rangle \approx 8$ m/day.

2.2. Lagrangian Particle Tracking

We discretize Equation 2 as

$$u_n^i = \frac{(m_p + m^*)\, u_n^{i-1} + \left(F_n^{GRP} + 6\pi\mu a_p v_n f_2\right)\Delta t}{m_p + m^* + \frac{1}{f_1} 6\pi\mu a_p \Delta t} \tag{6}$$

$$u_t^i = \frac{(m_p + m^*)\, u_t^{i-1} + \left(F_t^{GRP} + \frac{f_2}{f_4} 6\pi\mu a_p v_t\right)\Delta t}{m_p + m^* + \frac{1}{f_4} 6\pi\mu a_p \Delta t} \tag{7}$$

where subscripts n and t refer to the normal and tangential direction with respect to the nearest solid surface, respectively. f_1, f_2, f_3, and f_4 are universal hydrodynamic functions. $F_n^{GRP} = F_n^{EDL} + F_n^{V\,DW} + F_n^B$ and $F_t^{GRP} = F_t^B$ are the group of forces in normal and tangential directions, respectively, and a_p is the colloid radius. The derivation of Equations 6 and 7 and expressions for the universal hydrodynamic functions are detailed in Ma et al. (2009). The colloid velocity vector (u_n, u_t) at time step $i - 1$ is used to obtain the velocity vector at i. We apply bi-linear interpolation to calculate the normal and tangential fluid velocity components (v_n, v_t) within the numerical mesh. A challenge in applying Equations 6 and 7 lies in choosing the time step, especially, at a low separation distance between the colloid and the nearest solid surface, that is, less than 200 nm (herein referred to as NSZ). EDL and VDW forces change drastically when colloids enter the NSZ. Large time steps will allow the particle to pass the repulsive barrier without noticing it. However, the time step should be larger than the particle momentum relaxation time ($dt_{M\,RT} = m_p/6\pi\mu a_p$) to maintain uncorrelated (random) motion (T. Li & Raizen, 2013). We apply an adaptive time step algorithm to maintain the time step between 10 and 1,000 $dt_{M\,RT}$ as suggested by Pazmino, Trauscht, Dame, and Johnson (2014). Once a particle's velocity is calculated its position ($\boldsymbol{x}$) is updated via

$$\boldsymbol{x}^i = \boldsymbol{x}^{i-1} + \boldsymbol{u}^{i-1}\Delta t \tag{8}$$

Figure 2 shows an example of colloid trajectories in our complex geometry using the above described mechanistic particle tracking method.

3. Results and Discussion

Our simulations reflect a range of colloid sizes, d_p (0.3, 1.1, 2, and 4.4 μm), fluid average velocities, $\langle \boldsymbol{v} \rangle$ (2, 4, 8, 16, and 32 m/day), and ionic strengths, IS (6 and 20 mM) to test the effect of uniform and flux-weighted injection on colloid transport and deposition. We consider characteristic lengths of 100 μm (channel width), 300 μm (grain size), and 200 μm (grain size) in our Poiseuille flow, homogeneous geometry, and complex geometries cases, respectively. This yields Re numbers ranging between 0.0023 and 0.11. In many natural environments, groundwater flow velocities can fall below 1 m/day. However, higher velocities are commonly employed in colloid transport experiments, several of which motivate our work. We selected fluid velocities in line with those used in real experiments. Similarly, IS values can vary significantly outside the considered range and our was chosen based on ranges to be consistent with experiments such as those by X. Li et al. (2004) and X. Li and Johnson (2005).

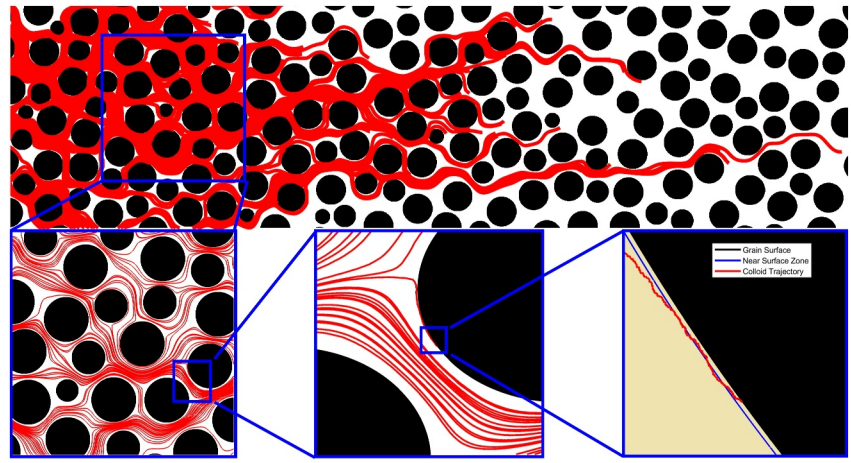

Figure 2. An example depiction of colloid trajectories using mechanistic pore-scale simulations highlighting different scales.

3.1. Colloid Retention in Poiseuille Flow Under Favorable Conditions

For the case of Poiseuille flow, colloids are injected based on uniform and flux-weighted distributions along the inlet of the domain. Then, Equations 6 and 7 are used to update colloid positions. Equation 5 is used to calculate the tangential fluid velocity component (v_t, along the flow direction and tangential to the channel walls) while the normal fluid velocity component (v_n) is zero (there is no flux in the normal direction to walls). We consider favorable conditions where colloids attach to both the top and bottom walls of the domain. By applying favorable conditions in Poiseuille's flow, all colloids entering the NSZ become attached. Consequently, the number of retained colloids remains unaffected by the IS. To validate this, we conducted simulations using two different IS values (6 and 20 mM), yielding similar results in terms of the number of retained colloids and the RP shape.

Figure 3 illustrates the distinction between uniform and flux-weighted injection modes, using mean fluid velocities ranging from 2 to 32 m/day and 2 μm colloids. In each injection mode, a total of $3.84{*}10^5$ colloids are injected. The uniform injection mode results in multi-exponential RPs (Figure 3a), while the flux-weighted injection mode displays a nonmonotonic shape for various fluid velocities (Figure 3b), with the degree of nonmonotonicity increasing with fluid speed.

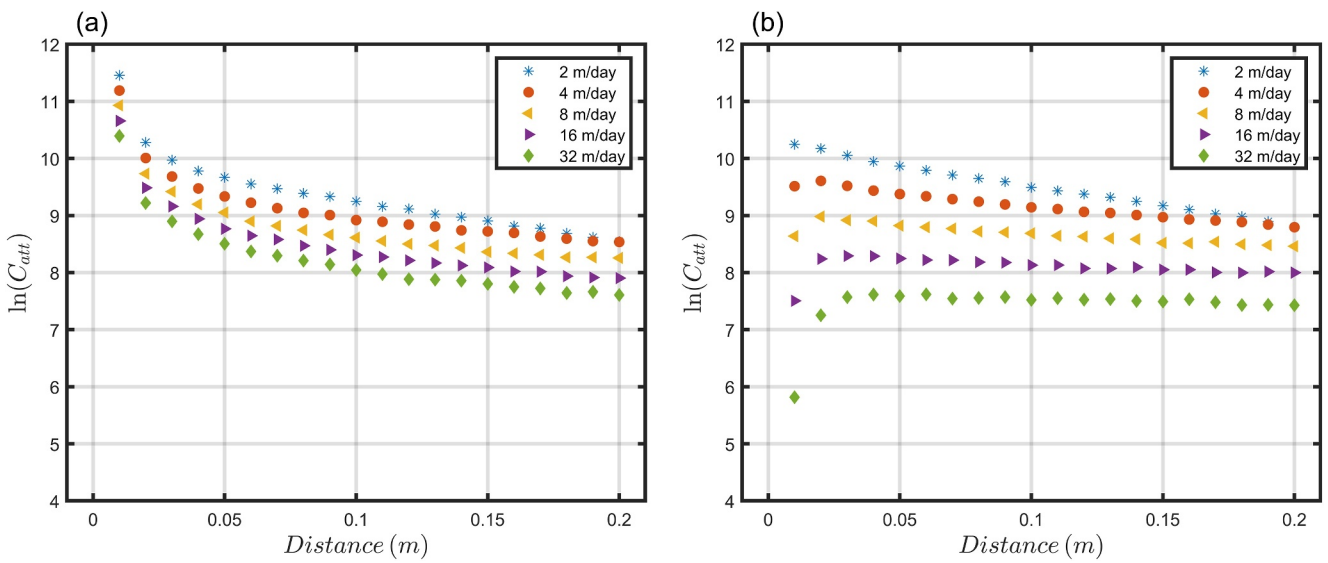

Figure 3. Retention profiles in Poiseuille's flow case for 2 μm colloids using a range of average fluid velocities ($\langle \boldsymbol{v} \rangle$ = 32, 16, 8, 4, and 2 m/day). (a) Uniform injection mode. (b) Flux-Weighted injection mode.

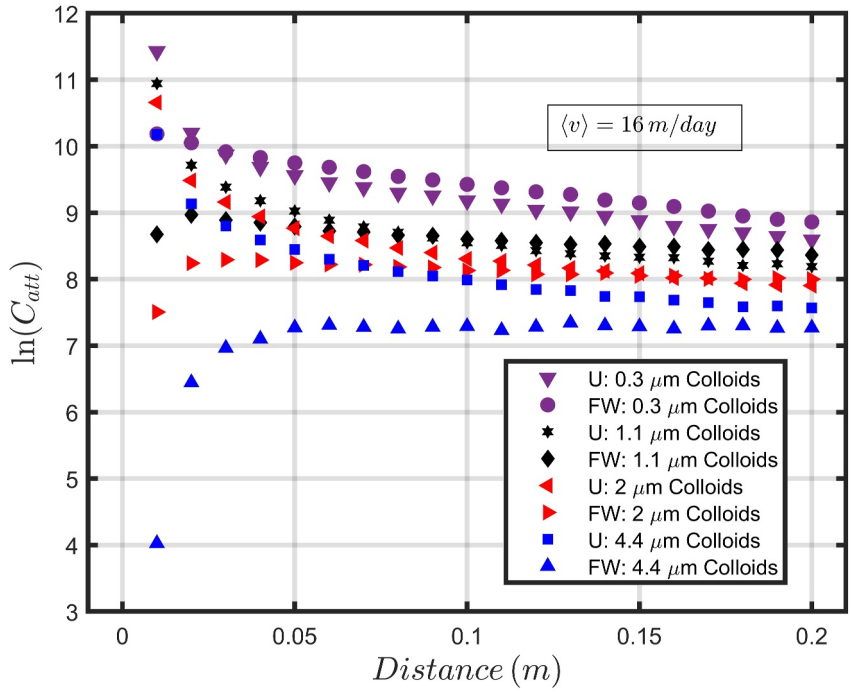

Figure 4. Retention profiles in Poiseuille's flow case under uniform and flux-weighted injection modes for different colloid sizes using average fluid velocity of 16 m/day.

The inherent relationship between the initial injection mode and the shape variation of the RP is primarily determined by the availability of colloids close to the NSZ at the domain's inlet. In the case of uniform injection mode, colloids are evenly distributed along the inlet injection line, ensuring a balanced proportion in both high and low-flux regions. This uniform distribution ensures colloids' proximity to the walls and facilitates their subsequent attachment within a short distance leading to (a sharp decrease in the number of attachments at the near-inlet portion of the RP). In contrast, the flux-weighted injection mode introduces a significantly reduced number of colloids in the low flux regions, which are situated in close proximity to the walls. Consequently, this reduction leads to a decrease in the number of attachments at the domain's inlet. However, through the processes of transverse diffusion, after traveling a certain distance, more colloids gradually approach the walls, leading to an increase in the number of attachments. In both injection modes, the fluid velocity plays a crucial role in determining the distance colloids must travel before getting closer to the walls and entering the NSZ. This is responsible for the observation of different slopes in the near-inlet portion of the RPs depicted in Figure 3. Furthermore, both injection modes exhibit an apparent increase in the number of attachments as the fluid velocity decreases, which aligns with findings from relevant literature (X. Li & Johnson, 2005; X. Li et al., 2004).

The shape of the RP is, also, influenced by the colloid size (X. Li & Johnson, 2005; X. Li et al., 2004; Tong & Johnson, 2007). In Figure 4, RPs are depicted for a range of colloid sizes that were injected using both uniform and flux-weighted injection distributions in Poiseuille flow. A specific fluid velocity of 16 m/day is employed for four different colloid sizes: 0.3, 1.1, 2, and 4.4 μm. As expected, since gravitational settling effects are neglected in our 2D simulations, the number of retained colloids decreases with increasing particle size (Tong & Johnson, 2007). This can be attributed to the influence of the diffusion force on the attachment process. In the case of Poiseuille flow, the streamlines follow a linear path extending from the inlet to the outlet of the domain. Colloids injected outside the NSZ can only be deviated from their streamlines by diffusion. In the absence of diffusion effects, only those colloids injected within the NSZ, where the EDL and VDW forces are significant, will attach. Hence, the diffusion force plays a vital role in determining how quickly colloids can migrate to the NSZ and thus influences the number of attached colloids. Since smaller colloids (0.3 μm) experience a stronger diffusion force, they reach the domain walls more quickly when compared to larger colloids. This trend is evident in Figure 4 for both injection modes. Under the flux-weighted injection mode, the increase in attachments in the near-inlet portion occurs over a shorter transport distance for smaller colloids. Consequently, uniformly injected smaller

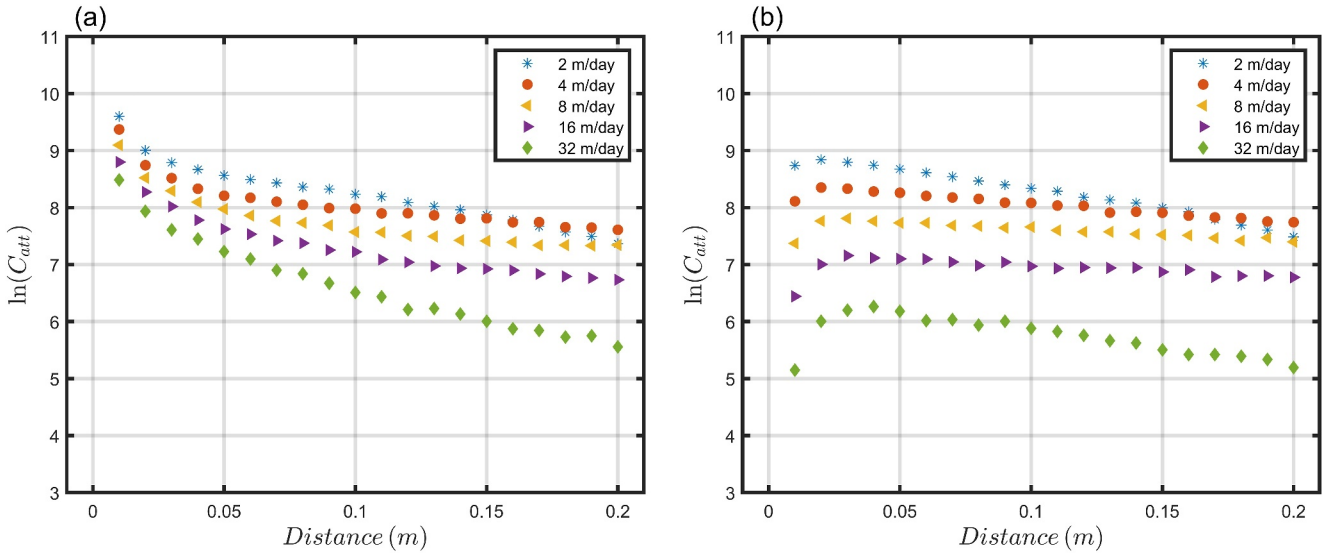

Figure 5. Retention profiles in homogeneous symmetrical geometry for 1.1 μm colloids using a range of average fluid velocities ($\langle v \rangle$ = 32, 16, 8, 4, and 2 m/day), surface coverage of 0.15% and ionic strength of 20 mM. (a) Uniform injection mode. (b) Flux-Weighted injection mode.

colloids result in the steepest slope near the inlet portion of the multi-exponential RP and a stronger non-monotonic signature emerges for larger colloids for the flux weighted scenario.

3.2. Colloid Retention in 2D Porous Media Under Favorable and Unfavorable Conditions

While interesting and serving the purpose of highlighting specific physical mechanisms, the Poiseuille flow case is highly idealized and the straight nature of the streamlines is not reflective of flow through real porous media. To validate our findings for both injection modes, we implemented flow and transport under favorable and unfavorable conditions on our homogeneous symmetrical geometry (refer to Figure 1a) and complex periodic geometries (refer to Figures 1b and 1c). The introduction of surface heterogeneity allowed us to simulate unfavorable scenarios with attachment in porous media by dispersing nanosized heterodomains across the grain surfaces (Pazmino, Trauscht, Dame, & Johnson, 2014; Trauscht et al., 2015). Since our simulations were conducted in a two-dimensional context, we represented the heterodomains as uniformly distributed arcs along the collector perimeter. Additionally, we use 0.15%, 0.23%, and 0.45% surface coverage (SCOV) of the total grains' surface area with heterodomains, each measuring 240 nm in length. A total of $1.92{*}10^5$ colloids were injected, employing both initial injection modes, and utilizing the same mean fluid velocities and colloid sizes as those employed in the Poiseuille flow case. To account for the unfavorable conditions, we incorporated two distinct ionic strengths (6 and 20 mM).

3.2.1. Homogeneous Symmetric Geometry

Figure 5 shows RPs for colloids injected in the homogeneous symmetric geometry (Figure 1a) using unfavorable conditions with IS of 20 mM and SCOV of 0.15%. It demonstrates similar behaviors to our Poiseuille flow case for both injection modes. The uniform injection mode (Figure 5a) and the flux-weighted injection mode (Figure 5b) yielded multi-exponential and nonmonotonic RPs, respectively, for various fluid velocities, aligning well with the observed trends in Figure 3. Furthermore, Figure 6a illustrates the RPs under both injection modes for different colloid sizes, demonstrating similar findings to those presented in Figure 4. The uniform and flux-weighted injection modes were also examined for two different IS values, as shown in Figure 6b. The simulations were conducted using a mean fluid velocity of 2 m/day and 4.4 μm colloids. Interestingly, our findings indicate that altering the IS does not affect the emergence of multi-exponential and nonmonotonic RPs under the uniform and flux-weighted injection modes, respectively. It is worth noting that increasing the IS value compresses the EDL repulsion, reduces the repulsive barrier, and leads to a higher number of attachments under unfavorable conditions (X. Li & Johnson, 2005; Tong & Johnson, 2007). Consequently, this might affect the attachment rate at the near-inlet portion of the domain for both injection modes (Figure 6b). However, it is important to emphasize

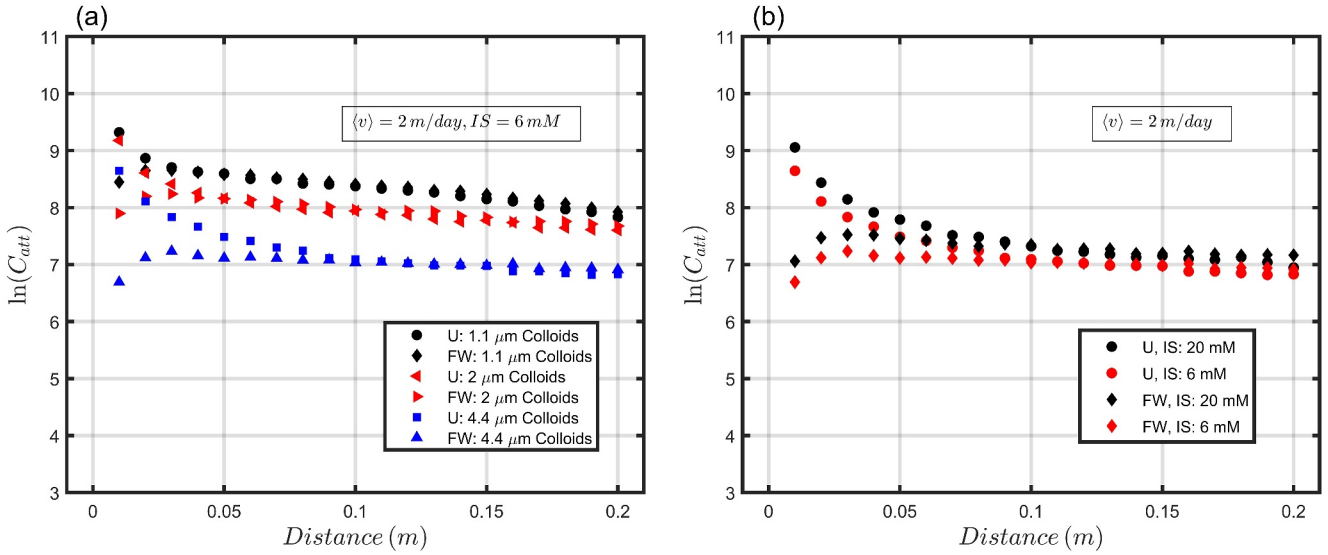

Figure 6. Retention profiles in homogeneous symmetrical geometry under uniform and flux-weighted injection modes using average fluid velocity $\langle \boldsymbol{v} \rangle$ of 2 m/day and surface coverage of 0.15%. (a) Uniform versus Flux-weighted injection for different colloid sizes (1.1, 2, and 4.4 μm) at an ionic strength (IS) of 6 mM. (b) Uniform versus Flux-weighted injection for different ionic strengths (6 and 20 mM) for 4.4 μm colloids.

that this variation in attachment rates does not impact our finding of obtaining multi-exponential and non-monotonic RPs for the uniform and flux-weighted injection modes, respectively.

To investigate whether the simulated anomalous transport behavior, characterized by multi-exponential and nonmonotonic RPs, is unique to unfavorable conditions, we conducted simulations under both favorable and unfavorable conditions while varying the values of SCOV, as depicted in Figure 7. In both injection modes, we employed 2 μm colloids, 6 mM IS, and $\langle \boldsymbol{v} \rangle$ of 16 m/day. Figure 6a, demonstrates that even under favorable conditions using the uniform injection mode, the multi-exponential RPs can still be observed. Furthermore, nonmonotonic RPs emerge when employing the flux-weighted injection method under favorable conditions, as shown in Figure 7b. These findings show that such anomalous transport is not unique to unfavorable conditions. It also emphasizes the significance of the initial injection conditions on colloid transport and deposition.

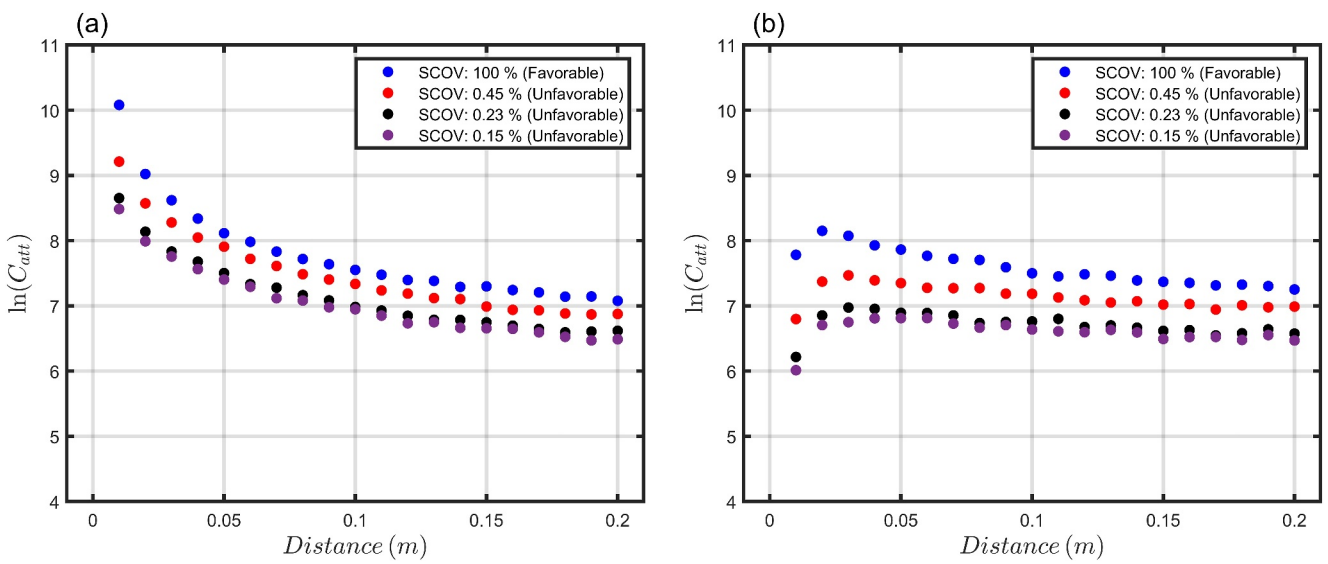

Figure 7. Retention profiles in homogeneous symmetrical geometry using average fluid velocity $\langle \boldsymbol{v} \rangle$ of 16 m/day and surface coverage of 0.15%, 0.23%, 0.45%, and 100% (favorable) using 2 μm colloids and 6 mM ionic strength (a) Uniform injection and (b) Flux-Weighted injection.

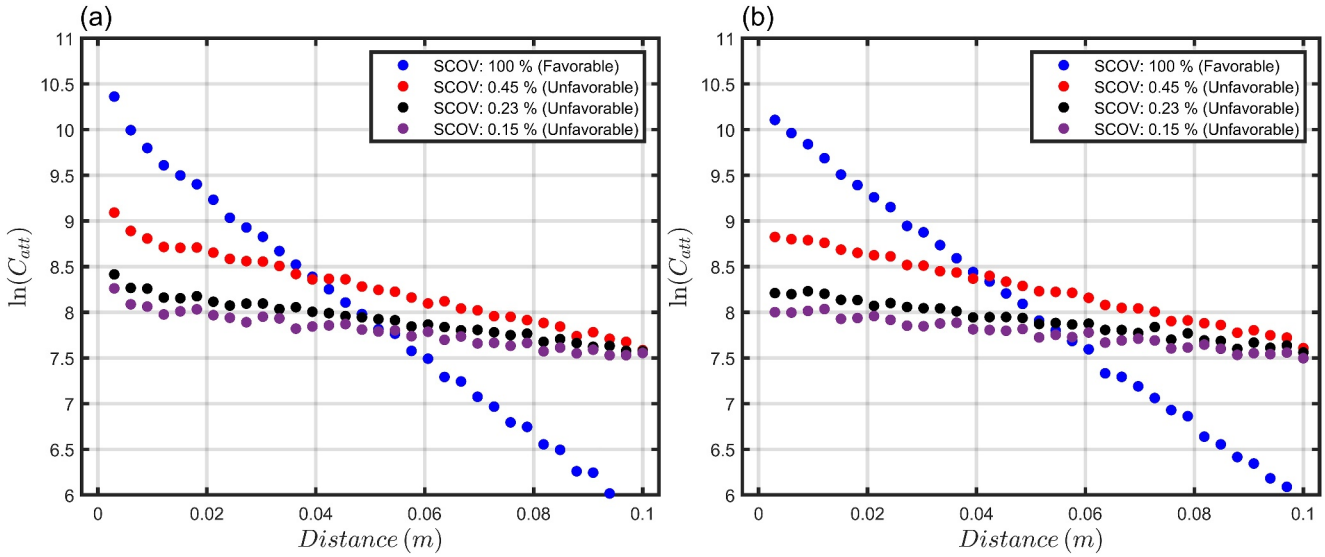

Figure 8. Retention profiles in Complex geometry using average fluid velocity $\langle v \rangle$ of 4 m/day and surface coverage of 0.15%, 0.23%, 0.45%, and 100% (favorable) using 1.1 μm colloids and 6 mM ionic strength (a) Uniform injection and (b) Flux-Weighted injection.

Additionally, this figure highlights the influence of SCOV on the shape of the RPs and the total number of retained colloids. The impact of SCOV on the rate of the near-inlet portion of both the multi-exponential and nonmonotonic RPs is also evident.

3.2.2. Colloid Retention in 2D Complex Geometry

To achieve a representation of RPs in more realistic porous media, we also studied a more complex 2D geometry (Figure 1b). Uniform and flux-weighted injection modes under favorable and unfavorable conditions were conducted using various values of SCOV, consistent with those employed in the homogeneous symmetric geometry. Furthermore, an IS of 6 mM and $\langle v \rangle$ of 4 m/day have been utilized. When colloids were injected uniformly (Figure 8a), RPs exhibited multi-exponential profiles. However, in cases characterized by the lowest SCOV values (representing unfavorable conditions), the multi-exponential RP shape is more pronounced. Conversely, when the injection mode was flux-weighted, the multi-exponential RP disappeared; however, unlike our previous test cases a nonmonotonic RP shape does not emerge, either for favorable or unfavorable conditions. Instead, a single-rate exponential decay emerged. These findings demonstrate that the initial injection mode does influence the shape of simulated RPs. However, it is not the only factor impacting it and that perhaps in complex geometries its influence is less pronounced than other factors, particularly given that geometry is known to play an important role in characterizing RPs (Johnson et al., 2018).

3.2.3. Colloid Retention in 2D Complex Geometry With Preferential Flow Pathways

One of the major differences between our two simple flows and the complex geometry discussed in the previous section is the absence of persistent high flux preferential flow paths. So, given the ubiquity of preferential flows in real environmental settings (Morales et al., 2010), we asked if the presence of such a preferential flow path in a more complex geometry can give rise to non-monotonic RPs. This motivated our fourth and final geometry (depicted in Figure 1c). Figure 9b illustrates the disparity in velocity magnitude distribution between the complex geometry (Figure 1b) and those augmented with preferential flow pathways (Figure 1c). The incorporation of preferential flow pathways yields both more elevated and diminished velocities compared to geometries lacking such defined pathways. This observation underscores the significant influence of preferential flow pathways on velocity distribution within complex geometries.

Under the flux-weighted injection initial condition for this geometry, with an IS of 20 mM and $\langle v \rangle$ of 8 m/day, under both favorable and unfavorable conditions, we do indeed observe the emergence of nonmonotonic RPs, as illustrated in Figure 9. A flux-weighted injection delivers a larger quantity of colloidal particles to the high-flux regions, which correspond to the preferential flow pathways. Consequently, a considerable portion of these

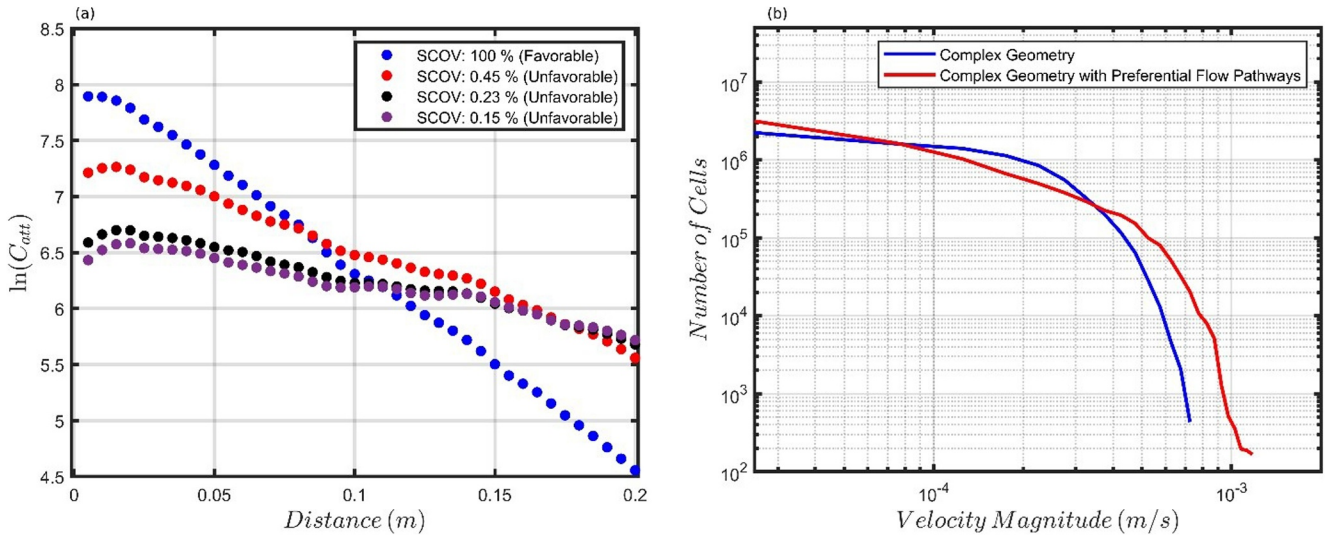

Figure 9. Effects of the preferential flow pathway on colloid retention and velocity distribution. (a) Retention profiles in Complex geometry with preferential flow pathways using flux-weighted injection mode, average fluid velocity $\langle v \rangle$ of 8 m/day and surface coverage of 0.15%, 0.23%, 0.45%, and 100% (favorable), 1.1 μm colloids and 6 mM ionic strength (b) velocity magnitude distribution among all fluid cells in complex geometry (blue) V.S. complex geometry with preferential flow pathways (red).

colloids exhibit relatively prolonged displacement along the preferential flows before any significant interaction with collector grains. After some time, particles eventually initiate interactions with collector grains, and a non-monotonic RP emerges. Importantly, this behavior manifests under both favorable and unfavorable conditions, although its manifestation is more pronounced in the latter scenario.

3.3. Systematic Analysis of Length Scales

We demonstrate the significant influence of the initial injection conditions, both uniform and flux-weighted, on the resulting RPs across a spectrum of flow geometries. Furthermore, we observe that the impact of these initial injection conditions diminishes with increasing flow complexity, as illustrated in Figure 8. This diminishment is attributed to the flow complexity mitigating the effects of the initial conditions and large velocity differences driving spreading, thus leading to a rapid convergence of RPs with different initial conditions downstream. However, it is not immediately obvious what sets this convergence scale (e.g., Figures 3, 5, and 8). To address this variability we consider two pertinent timescales: the diffusion timescale $\left(t_D = l_c^2/D\right)$ and the advection (velocity decorrelation) timescale ($t_a = l_c/v_c$). Here, l_c denotes the characteristic length, approximated as the average collector size (200 μm), and v_c the characteristic fluid velocity. Although both timescales are important they compete in setting asymptotic behavior. In our cases, the advection timescale is typically the faster more important one due to low magnitudes of D for colloids ($\sim 10^{-13}$ m^2/s). In our cases the advection timescale is about five orders of magnitude smaller than the diffusion timescale. Figure 10 depicts the residence time distribution, normalized with the advection timescale, for 1.1 μm colloids injected via uniform and flux-weighted methods, employing average fluid velocities of 2 and 8 m/day under unfavorable conditions in the case of Poiseuille flow (Figure 10a) and the homogeneous symmetric geometry (Figure 10b). For Poiseuille flow both injection modes converge at a later time ($\sim 250\ t_a$) compared to the homogeneous symmetrical geometry ($\sim 150\ t_a$), corroborating our hypothesis regarding the impact of increasing complexity on the persistence of initial injection conditions downstream. As complexity in the hosting medium increases, we anticipate a shorter distance/time for the effects of the initial conditions to wash out. Figure 11 illustrates the resulting RP using both uniform and flux-weighted conditions within the complex geometry (Figure 1b) under unfavorable conditions (0.15% SCOV), employing a fluid velocity of 4 m/day, equivalent to the characteristic velocity (v_c). A disparity between these profiles is observed near the inlet, attributed to the influence of the initial injection conditions. However, with increasing downstream distance, the profiles for both injection modes rapidly converge, thereby diminishing the influence of the initial injection condition more quickly than the less complex geometries (Figure 10). As depicted in Figure 11 (inset), the convergence of RPs employing uniform and flux-weighted

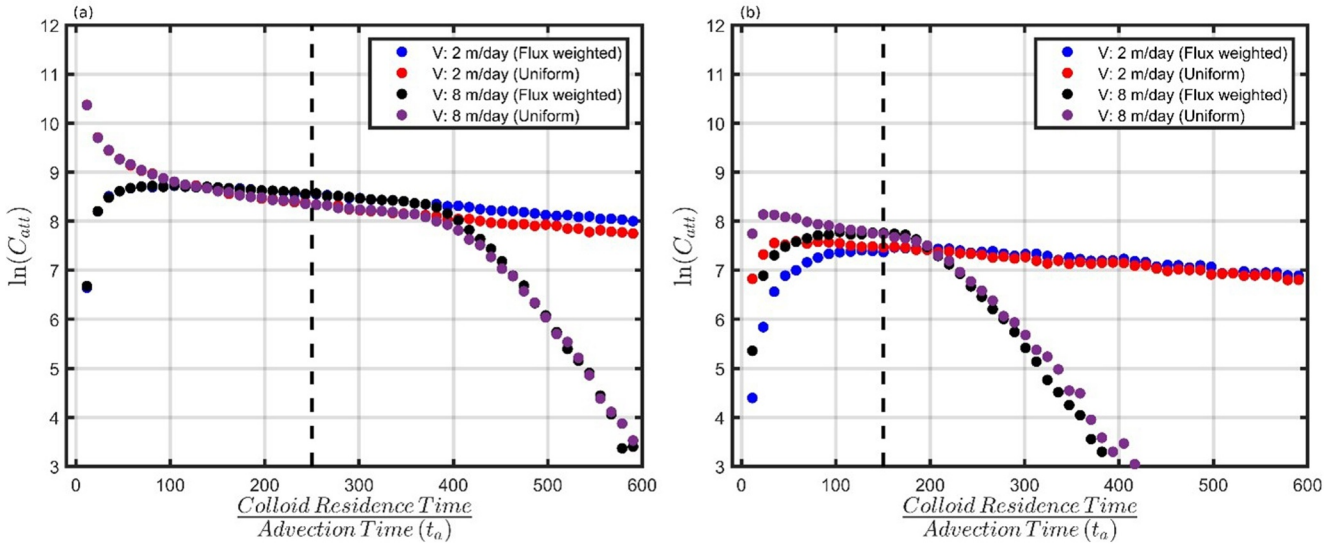

Figure 10. Normalized residence time distributions for colloids retained under unfavorable conditions, comparing uniform and flux-weighted injection conditions. Average fluid velocities $\langle v \rangle$ of 2 and 8 m/day and surface coverage of 0.15 are utilized with 1.1 μm colloids and 6 mM ionic strength. Time is normalized to the advection timescale, t_a, and the dashed line indicates the normalized time at which both injection modes converge. (a) Poiseuille's flow and (b) Homogeneous symmetrical geometry.

injection occurs after approximately 40 grains, equivalent to 40 t_a, again indicating the diminishing effect of the initial injection conditions. These findings align with similar trends documented in fractured networks (Kang et al., 2017).

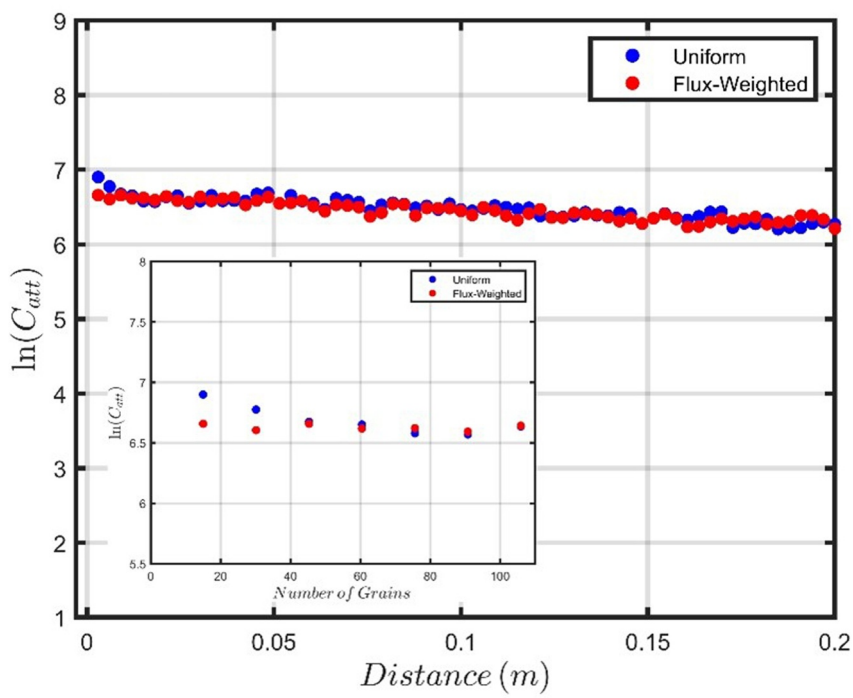

Figure 11. Retention profiles in complex geometry under unfavorable conditions for uniform (red) and flux-weighted (blue) injection conditions using average fluid velocity $\langle v \rangle$ of 4 m/day and surface coverage of 0.15 with 1.1 μm colloids and 6 mM ionic strength. Inset: colloid retention using uniform and flux-weighted injection as a function of the number of grains passed along the flow direction.

To date, the bulk of research in this field focuses on explaining the anomalous transport in colloids among identical individuals by the presence of the repulsive energy barrier (unfavorable conditions) between the colloid and the grains of the hosting medium. However, our investigation primarily concentrates on elucidating the influence of flow geometry itself on the observation of anomalous colloid retention, regardless of the presence or absence of the energy-repulsive barrier. As discussed herein, simpler geometries such as Poiseuille flow and homogeneous symmetric geometry necessitate greater distance/time to attenuate the effect of the initial injection condition, thereby enabling the observation of anomalous transport even under favorable conditions. Conversely, with increasing complexity, resembling geometries employed in real laboratory settings, the impact of the initial injection condition diminishes rapidly over a shorter distance/time. Therefore, the effect of the initial injection condition is more pronounced in simpler geometries; as the complexity of the hosting medium escalates, this effect vanishes, emphasizing the pivotal role of geometry itself in manifesting the impact of initial injection conditions on colloid retention, regardless of the presence or absence of the energy repulsive barrier. Also, we are not aiming to claim that uniform and flux-weighted injections are the main drivers in obtaining multi-exponential and nonmonotonic RPs, respectively. Rather, our focus is to highlight the potential effects of initial injection conditions among various flow geometries and that caution should be taken in accounting for their influence when needed. Furthermore, Although our simulations are conducted in 2D, we anticipate similar observations in 3D geometry. The variation in fluid velocity near the inlet and throughout the domain also persists in 3D, emphasizing the disparity between both initial injection conditions. However, simulating colloid retention under unfavorable conditions in 3D presents distinct challenges compared to 2D simulations and is left for future work.

4. Summary and Conclusions

The influence of the initial injection condition on colloid transport and retention was investigated in this study, employing both uniform and flux-weighted distributions for the initial colloid locations. Various domains, including Poiseuille flow between two parallel plates, flow in a homogeneous symmetric geometry, and flow in two more complex geometries (Figure 1), were chosen, encompassing different ranges of fluid velocity, colloid size, and IS. The results clearly demonstrated the significant role played by the choice of initial injection mode in shaping the RPs of the colloids. The uniform injection modes displayed multi-exponential RPs, while the flux-weighted injection translated to nonmonotonic RPs in Poiseuille flow and the homogeneous symmetric geometry. In the more complex geometry (without obvious preferential flow pathways (Figure 1b), the uniform injection yielded multi-exponential RPs, while the flux-weighted injection displayed a single rate exponential decay and no evidence of non-monotonic RPs was found. However, when we considered a similar complex geometry, but with a strong preferential flow path, nonmonotonic RPs (Figure 9) emerged when applying a flux-weighted injection (Figure 1c). Given how common preferential flows are in real systems knowledge of this has important implications for experimental design and potentially interpretation of experimental data. In terms of the distinction between favorable, unfavorable conditions, and the two injection modes, our findings reveal that the flux-weighted initial condition yields a non-monotonic shape, while the uniform injection mode manifests multi-exponential shapes in simpler geometries, such as Poiseuille flow and our homogeneous symmetric geometry, under favorable conditions. While exploring more complex geometries, it is plausible to correlate the contrast between initial injection conditions and favorable versus unfavorable conditions. However, such an endeavor exceeds the scope of this current study, which primarily aims to elucidate the impact of the initial injection condition across diverse flow geometries.

Furthermore, the impact of other parameters, such as fluid velocity, colloid size, and IS, was observed to alter the attachment rate near the inlet region of the domain and the total number of attachments within the domain, without affecting the qualitative transition between multi-exponential and nonmonotonic RPs significantly. Our findings reveal that multi-exponential and nonmonotonic simulated RPs can emerge under favorable conditions in contrast to reported experimental observations. Nevertheless, it is important to note that the selected injection mode ultimately determined the shape of the RPs. Taken together, our findings highlight the influence of the initial injection condition on colloid transport in porous media and offer a plausible explanation of one mechanism that contributes to observed anomalous transport behaviors. With this work we are not implying that all such observations to date are attributable to this, but rather highlighting that such mechanisms should be considered in interpretations as experimental initial conditions are difficult to control and known with a high degree of accuracy. To conclude, monitoring the initial injection condition in real experiments can prove challenging; it likely falls

somewhere between flux-weighted and uniform. Nonetheless, our findings underscore the importance of attending to the effects of initial injection conditions and their significant impact on shaping RPs.

Nomenclature

Re	Reynold's Number (-)
v_c	characteristic velocity (m/s)
l_c	characteristic length (m)
$\boldsymbol{v}$	fluid velocity vector (m/s)
$SCOV$	Surface Coverage by Het-domains (%)
IS	Ionic Strength (mM)
ν	Kinematic Viscosity (m^2/s)
μ	Dynamic Viscosity (Pa.s)
p	Pressure (Pa)
$\boldsymbol{u}$	Colloid Velocity Vector (m/s)
m_p	Colloid Mass (kg)
m^*	The Virtual Mass (kg)
t	Time (s)
Δt	Time Step (s)
dt_{MRT}	Momentum Relaxation Time (s)
$\boldsymbol{x}$	Colloid Position Vector (m)
F_D	Drag Force (N)
F_B	Brownian Force (N)
F_{EDL}	Electric Double Layers Force (N)
F_{VDW}	Van Der Waals Force (N)
d_p	Colloid Diameter (m)
a_p	Colloid Radius (m)
ρ_p	Colloid density (kg/m^3)
$\boldsymbol{x_o}$	Initial Colloids position (m)
$\rho(\boldsymbol{x_o})$	Colloid Distribution at the Inlet (-)
ψ_o	Injection Domain (-)
V_o	Injection Domain's Volume (m^3)
$\mathbb{I}_{\psi_o}(\boldsymbol{x_o})$	Indicator Function (-)
$v_o(\boldsymbol{x_o})$	Initial Colloids velocity (m/s)
d	Channel Width (m)
$\langle \boldsymbol{v} \rangle$	Average Fluid Velocity (m/s)
u_n	Colloid Velocity in the Normal Direction (m/s)
u_t	Colloid Velocity in the Tangential Direction (m/s)
v_n	Fluid Velocity in the Normal Direction (m/s)
v_t	Fluid Velocity in the Tangential Direction (m/s)
F_n^{GRP}	Group of Forces in the Normal Direction (N)
F_t^{GRP}	Group of Forces in the Tangential Direction (N)
f_1, f_2, f_3, and f_4	Universal Hydrodynamic Functions (-)
t_a	Advection Timescale (s)
t_D	Diffusion Timescale (s)
D	Diffusion Coefficient (m^2/s)

Abbreviations

RP	Retention Profile
FW	Flux-Weighted
U	Uniform
ENP	Engineered Nanoparticle

VDW	Van Der Waals
EDL	Electric Double Layers
DLVO	Derjaguin, Landau, Verwey, and Overbeek Theory
CFT	Colloid Filtration Theory
NSZ	Near Surface Zone

Data Availability Statement

The particle tracking model used in this manuscript for the calculation of the RPs is licensed under MIT license and published on Github https://github.com/BasharAlZghoul/The-One-Piece-for-Particle-Tracking (Al-Zghoul et al., 2023).

Acknowledgments
This work was supported by US National Science Foundation Projects EAR-1951676 and EAR-1951677.

References

Albinger, O., Biesemeyer, B. K., Arnold, R. G., & Logan, B. E. (1994). Effect of bacterial heterogeneity on adhesion to uniform collectors by monoclonal populations. *FEMS Microbiology Letters*, *124*(3), 321–326. https://doi.org/10.1016/0378-1097(94)00449-8

Al-Zghoul, B. M., & Abu-El-Sha'r, W. Y. (2020). New Gaussian plume equation for the impacts of dust storms on radionuclide transport. *Aerosol and Air Quality Research*, *20*(1), 119–127. https://doi.org/10.4209/AAQR.2019.09.0433

Al-Zghoul, B. M., Johnson, W. P., & Bolster, D. (2023). The one piece for particle tracking [Software]. *Zenodo*. https://doi.org/10.5281/zenodo.10068085

Amari, S. V., & Misra, R. B. (1997). Closed-form expressions for distribution of sum of exponential random variables. *IEEE Transactions on Reliability*, *46*(4), 519–522. https://doi.org/10.1109/24.693785

Bradford, S. A., Simunek, J., & Walker, S. L. (2006). Transport and straining of *E. coli* O157:H7 in saturated porous media. *Water Resources Research*, *42*(12), W12S12. https://doi.org/10.1029/2005WR004805

Bradford, S. A., Torkzaban, S., & Simunek, J. (2011). Modeling colloid transport and retention in saturated porous media under unfavorable attachment conditions. *Water Resources Research*, *47*(10), W10503. https://doi.org/10.1029/2011WR010812

Christopher, J. (2022). OpenFOAM the OpenFOAM foundation user guide. Retrieved from https://openfoam.org

Comolli, A., Hakoun, V., & Dentz, M. (2019). Mechanisms, upscaling, and prediction of anomalous dispersion in heterogeneous porous media. *Water Resources Research*, *55*(10), 8197–8222. https://doi.org/10.1029/2019WR024919

De Anna, P., Quaife, B., Biros, G., & Juanes, R. (2017). Prediction of the low-velocity distribution from the pore structure in simple porous media. *Physical Review Fluids*, *2*(12), 124103. https://doi.org/10.1103/PhysRevFluids.2.124103

Deb, D., & Chakma, S. (2022). *Colloid and colloid-facilitated contaminant transport in subsurface ecosystem—A concise review*. Springer Science and Business Media Deutschland GmbH. https://doi.org/10.1007/s13762-022-04201-z

Demmy, G., Berglund, S., & Graham, W. (1999). Injection mode implications for solute transport in porous media: Analysis in a stochastic Lagrangian framework. *Water Resources Research*, *35*(7), 1965–1973. https://doi.org/10.1029/1999WR900027

Derjaguin, B., & Landau, L. (1941). Theory of the stability of strongly charged Lyophobic Sols and of the adhesion of strongly charged particles in solutions of electrolytes. *Progress in Surface Science*, *43*(1–4), 30–59. https://doi.org/10.1016/0079-6816(93)90013-l

Ellmelech, M., & O'Mella, C. R. (1990). Kinetics of deposition of colloidal particles in porous media. *Environmental Science & Technology*, *24*(10), 1528–1536. https://doi.org/10.1021/es00080a012

Frampton, A., & Cvetkovic, V. (2009). Significance of injection modes and heterogeneity on spatial and temporal dispersion of advecting particles in two-dimensional discrete fracture networks. *Advances in Water Resources*, *32*(5), 649–658. https://doi.org/10.1016/j.advwatres.2008.07.010

Frampton, A., & Cvetkovic, V. (2011). Numerical and analytical modeling of advective travel times in realistic three-dimensional fracture networks. *Water Resources Research*, *47*(2), W02506. https://doi.org/10.1029/2010WR009290

Gondret, P., Lance, M., & Petit, L. (2002). Bouncing motion of spherical particles in fluids. *Physics of Fluids*, *14*(2), 643–652. https://doi.org/10.1063/1.1427920

Gotovac, H., Cvetkovic, V., & Andricevic, R. (2009). Flow and travel time statistics in highly heterogeneous porous media. *Water Resources Research*, *45*(7), W07402. https://doi.org/10.1029/2008WR007168

Gotovac, H., Cvetkovic, V., & Andricevic, R. (2010). Significance of higher moments for complete characterization of the travel time probability density function in heterogeneous porous media using the maximum entropy principle. *Water Resources Research*, *46*(5), W05502. https://doi.org/10.1029/2009WR008220

Hyman, J. D., & Dentz, M. (2021). Transport upscaling under flow heterogeneity and matrix-diffusion in three-dimensional discrete fracture networks. *Advances in Water Resources*, *155*, 103994. https://doi.org/10.1016/j.advwatres.2021.103994

Hyman, J. D., Painter, S. L., Viswanathan, H., Makedonska, N., & Karra, S. (2015). Influence of injection mode on transport properties in kilometer-scale three-dimensional discrete fracture networks. *Water Resources Research*, *51*(9), 7289–7308. https://doi.org/10.1002/2015WR017151

Johnson, W. P., Rasmuson, A., Pazmiño, E., & Hilpert, M. (2018). Why variant colloid transport behaviors emerge among identical individuals in porous media when colloid-surface repulsion exists. *Environmental Science and Technology*, *52*(13), 7230–7239. https://doi.org/10.1021/acs.est.8b00811

Kang, P. K., Dentz, M., Le Borgne, T., Lee, S., & Juanes, R. (2017). Anomalous transport in disordered fracture networks: Spatial Markov model for dispersion with variable injection modes. *Advances in Water Resources*, *106*, 80–94. https://doi.org/10.1016/j.advwatres.2017.03.024

Klaine, S. J., Alvarez, P. J., Batley, G. E., Fernandes, T. F., Handy, R. D., Lyon, D. Y., et al. (2008). Nanomaterials in the environment: Behavior, fate, bioavailability, and effects. *Environmental Toxicology and Chemistry: International Journal*, *27*(9), 1825–1851. https://doi.org/10.1897/08-090.1

Li, T., & Raizen, M. G. (2013). Brownian motion at short time scales. *Annalen der Physik*, *525*(4), 281–295. https://doi.org/10.1002/andp.201200232

Li, X., & Johnson, W. P. (2005). Nonmonotonic variations in deposition rate coefficients of microspheres in porous media under unfavorable deposition conditions. *Environmental Science and Technology*, *39*(6), 1658–1665. https://doi.org/10.1021/es048963b

Li, X., Scheibe, T. D., & Johnson, W. P. (2004). Apparent decreases in colloid deposition rate coefficients with distance of transport under unfavorable deposition conditions: A general phenomenon. *Environmental Science and Technology*, *38*(21), 5616–5625. https://doi.org/10.1021/es049154v

Liang, Y., Bradford, S. A., Simunek, J., Heggen, M., Vereecken, H., & Klumpp, E. (2013). Retention and remobilization of stabilized silver nanoparticles in an undisturbed loamy sand soil. *Environmental Science and Technology*, *47*(21), 12229–12237. https://doi.org/10.1021/es402046u

Ma, H., Pedel, J., Fife, P., & Johnson, W. P. (2009). Hemispheres-in-cell geometry to predict colloid deposition in porous media. *Environmental Science and Technology*, *43*(22), 8573–8579. https://doi.org/10.1021/es901242b

Malgaresi, G., Collins, B., Alvaro, P., & Bedrikovetsky, P. (2019). Explaining non-monotonic retention profiles during flow of size-distributed colloids. *Chemical Engineering Journal*, *375*, 121984. https://doi.org/10.1016/j.cej.2019.121984

Molnar, I. L., Johnson, W. P., Gerhard, J. I., Willson, C. S., & O'Carroll, D. M. (2015). Predicting colloid transport through saturated porous media: A critical review. *Water Resources Research*, *51*(9), 6804–6845. https://doi.org/10.1002/2015WR017318

Morales, V. L., Parlange, J. Y., & Steenhuis, T. S. (2010). Are preferential flow paths perpetuated by microbial activity in the soil matrix? A review. *Journal of Hydrology*, *393*(1–2), 29–36. https://doi.org/10.1016/j.jhydrol.2009.12.048

Nelson, K. E., & Ginn, T. R. (2011). New collector efficiency equation for colloid filtration in both natural and engineered flow conditions. *Water Resources Research*, *47*(5), W05543. https://doi.org/10.1029/2010WR009587

Pazmino, E., Trauscht, J., Dame, B., & Johnson, W. P. (2014). Power law size-distributed heterogeneity explains colloid retention on soda lime glass in the presence of energy barriers. *Langmuir*, *30*(19), 5412–5421. https://doi.org/10.1021/la501006p

Pazmino, E., Trauscht, J., & Johnson, W. P. (2014). Release of colloids from primary minimum contact under unfavorable conditions by perturbations in ionic strength and flow rate. *Environmental Science and Technology*, *48*(16), 9227–9235. https://doi.org/10.1021/es502503y

Petosa, A. R., Jaisi, D. P., Quevedo, I. R., Elimelech, M., & Tufenkji, N. (2010). Aggregation and deposition of engineered nanomaterials in aquatic environments: Role of physicochemical interactions. *Environmental Science and Technology*, *44*(17), 6532–6549. https://doi.org/10.1021/es100598h

Puyguiraud, A., Gouze, P., & Dentz, M. (2019a). Stochastic dynamics of Lagrangian pore-scale velocities in three-dimensional porous media. *Water Resources Research*, *55*(2), 1196–1217. https://doi.org/10.1029/2018WR023702

Puyguiraud, A., Gouze, P., & Dentz, M. (2019b). Upscaling of anomalous pore-scale dispersion. *Transport in Porous Media*, *128*(2), 837–855. https://doi.org/10.1007/s11242-019-01273-3

Rajagopalan, R., & Tien, C. (1976). Trajectory analysis of deep-bed filtration with the sphere-in-cell porous media model. *AIChE Journal*, *22*(3), 523–533. https://doi.org/10.1002/aic.690220316

Ryan, J. N., & Elimelech, M. (1996). COLLOIDS A AND Colloids and Surfaces SURFACES ELSEVIER Colloid mobilization and transport in groundwater (Vol. 107).

Shapiro, A. A., & Bedrikovetsky, P. G. (2008). Elliptic random-walk equation for suspension and tracer transport in porous media. *Physica A: Statistical Mechanics and its Applications*, *387*(24), 5963–5978. https://doi.org/10.1016/j.physa.2008.07.013

Skoge, M., Donev, A., Stillinger, F. H., & Torquato, S. (2006). Packing hyperspheres in high-dimensional Euclidean spaces. *Physical Review E - Statistical, Nonlinear and Soft Matter Physics*, *74*(4), 041127. https://doi.org/10.1103/PhysRevE.74.041127

Taylor, W. L. (1953). "Cloze procedure": A new tool for measuring readability. *Journalism Quarterly*, *30*(4), 415–433. https://doi.org/10.1177/107769905303000401

Tong, M., & Johnson, W. P. (2007). Colloid population heterogeneity drives hyperexponential deviation from classic filtration theory. *Environmental Science and Technology*, *41*(2), 493–499. https://doi.org/10.1021/es061202j

Tong, M., Li, X., Brow, C. N., & Johnson, W. P. (2005). Detachment-influenced transport of an adhesion-deficient bacterial strain within water-reactive porous media. *Environmental Science and Technology*, *39*(8), 2500–2508. https://doi.org/10.1021/es049013t

Trauscht, J., Pazmino, E., & Johnson, W. P. (2015). Prediction of nanoparticle and colloid attachment on unfavorable mineral surfaces using representative discrete heterogeneity. *Langmuir*, *31*(34), 9366–9378. https://doi.org/10.1021/acs.langmuir.5b02369

Tufenkji, N., & Elimelech, M. (2004a). Correlation equation for predicting single-collector efficiency in physicochemical filtration in saturated porous media. *Environmental Science and Technology*, *38*(2), 529–536. https://doi.org/10.1021/es034049r

Tufenkji, N., & Elimelech, M. (2004b). Deviation from the classical colloid filtration theory in the presence of repulsive DLVO interactions. *Langmuir*, *20*(25), 10818–10828. https://doi.org/10.1021/la0486638

Verwey, E. J. W., & Overbeek, J. T. G. (1948). *Theory of the stability of lyophobic colloids*. Elsevier.

Wang, D., Ge, L., He, J., Zhang, W., Jaisi, D. P., & Zhou, D. (2014). Hyperexponential and nonmonotonic retention of polyvinylpyrrolidone-coated silver nanoparticles in an Ultisol. *Journal of Contaminant Hydrology*, *164*, 35–48. https://doi.org/10.1016/j.jconhyd.2014.05.007

Yao, K.-M., Habibian, M. T., & O'Melia, C. R. (1971). Current research water and waste water filtration: Concepts and applications. *Environmental Science & Technology*, *5*(11), 1105–1112. https://doi.org/10.1021/es60058a005

Yuan, H., & Shapiro, A. A. (2010). Modeling non-Fickian transport and hyperexponential deposition for deep bed filtration. *Chemical Engineering Journal*, *162*(3), 974–988. https://doi.org/10.1016/j.cej.2010.07.003

Yuan, H., & Shapiro, A. A. (2011). A mathematical model for non-monotonic deposition profiles in deep bed filtration systems. *Chemical Engineering Journal*, *166*(1), 105–115. https://doi.org/10.1016/j.cej.2010.10.036